

See discussions, stats, and author profiles for this publication at: <https://www.researchgate.net/publication/255984749>

# Novel 1,2,4-Thiadiazole Derivatives: Crystal Structure, Conformational Analysis, Hydrogen Bond Networks, Calculations, and Thermodynamic Characteristics of Crystal Lattices

ARTICLE *in* THE JOURNAL OF PHYSICAL CHEMISTRY B · AUGUST 2013

Impact Factor: 3.3 · DOI: 10.1021/jp405624e · Source: PubMed

---

CITATIONS

5

READS

44

## 6 AUTHORS, INCLUDING:



Artem Surov

Institute of Solution Chemistry of RAS

28 PUBLICATIONS 132 CITATIONS

[SEE PROFILE](#)



Pascal Roussel

National Graduate School of Engineering Che...

314 PUBLICATIONS 2,092 CITATIONS

[SEE PROFILE](#)



Idrissi Abdenacer

Université des Sciences et Technologies de Lill...

107 PUBLICATIONS 559 CITATIONS

[SEE PROFILE](#)



German L Perlovich

Institute of Solution Chemistry of RAS

142 PUBLICATIONS 1,479 CITATIONS

[SEE PROFILE](#)

# Novel 1,2,4-Thiadiazole Derivatives: Crystal Structure, Conformational Analysis, Hydrogen Bond Networks, Calculations, and Thermodynamic Characteristics of Crystal Lattices

Artem O. Surov,<sup>†</sup> Cong Trinh Bui,<sup>†,⊥</sup> Alexey N. Proshin,<sup>‡</sup> Pascal Roussel,<sup>§</sup> Abdenacer Idrissi,<sup>||</sup> and German L. Perlovich<sup>\*,†,‡</sup>

<sup>†</sup>Institute of Solution Chemistry, Russian Academy of Sciences, 153045 Ivanovo, Russia

<sup>‡</sup>Institute of Physiologically Active Compounds, Russian Academy of Sciences, 142432 Chernogolovka, Russia

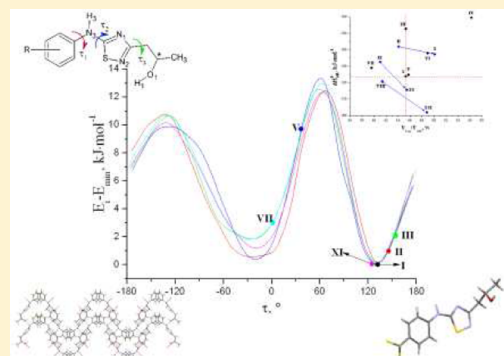
<sup>§</sup>UCCS, UMR 8181, University des Sciences et Technologies de Lille-1, Lille, France

<sup>||</sup>LASIR, UMR 8516, University des Sciences et Technologies de Lille-1, Lille, France

<sup>⊥</sup>Ivanovo State University of Chemical Sciences and Technology, 153460 Ivanovo, Russia

## Supporting Information

**ABSTRACT:** The results of X-ray crystallographic and computational studies of twelve 1,2,4-thiadiazole derivatives are reported. The effect of orientation of different parts of the molecules on crystal organization and hydrogen bond network were studied. DFT calculations were carried out in order to explore conformational preferences of the molecules inside and outside of crystal environment. The role of hydrogen bonds was found to be essential for the stabilization of conformationally strained molecules as well as for the packing density of such molecules in a crystal. Thermodynamic aspects of sublimation processes of the studied compounds were analyzed using temperature dependencies of their vapor pressure. Thermophysical characteristics of the molecular crystals were obtained and compared with the sublimation enthalpy and the structural parameters. The influence of crystal structure features on the sublimation enthalpy and on the melting temperature was analyzed.



## 1. INTRODUCTION

Thiadiazoles represent an important class of heterocyclic compounds that exhibit different types of biological activity. In the past decade, a number of potent compounds based on thiadiazoles have been discovered.<sup>1</sup> Indeed, compounds containing a 1,2,4-thiadiazole fragment have anti-inflammatory,<sup>2,3</sup> antihypertensive,<sup>4</sup> antibacterial,<sup>5,6</sup> and anticonvulsant properties.<sup>7,8</sup> Furthermore, it has been confirmed that many thiadiazole-related compounds are potential drugs in the treatment of disorders of the central nervous system such as Alzheimer's disease due to the antioxidant properties, influence on muscarinic acetylcholine receptors,<sup>9</sup> and inhibition of acetylcholinesterase activity.<sup>10</sup> Compounds containing a 1,2,4-thiadiazole fragment also display high inhibitory activity against glycogen synthase kinase-3 $\beta$  and, therefore, can be used for treatment of neuropathology, disordered motor function, chronic inflammatory process, cancer, and diabetes of type II.<sup>11</sup> Recently, we have tested the ability of a wide range of structurally related phenyl derivatives of 1,2,4-thiadiazole to inhibit glutamate stimulated Ca uptake. As a result, such compounds are found to be active against the *N*-methyl-D-aspartate receptor which is responsible for the neuronal

signaling processes, memory consolidation, and synaptic plasticity.<sup>12</sup>

Although the receptor affinity in many cases is undoubtedly the key issue for potent drugs, other factors may be equally important for application *in vivo* such as solubility. Unfortunately, in many cases, this important aspect is subject to later studies in drug discovery and drug development research. Therefore, as most new drug candidates are in the first place only tested *in vitro*, one comes across an enormous number of new promising drug compounds of high receptor affinity with poor physicochemical material properties. This is a serious drawback for a drug candidate on its way to become a useful pharmaceutical agent, as it is hard to compensate for weak solubility properties even by using the most advanced drug delivery systems. It would be more efficient and economically beneficial to select candidates with less demanding solubility properties right at the beginning of the drug development research.

Received: June 7, 2013

Revised: August 12, 2013

Published: August 19, 2013

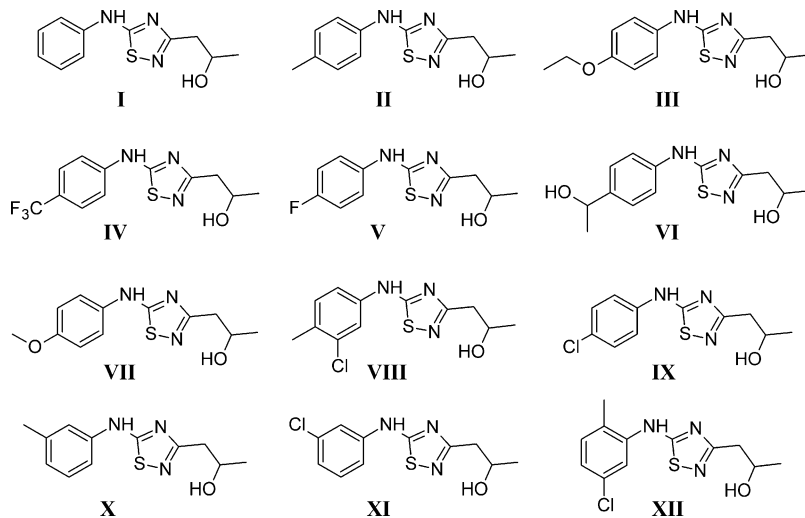


Figure 1. Molecular structures of the studied compounds.

Thermodynamically, solubility values are determined by sublimation characteristics of solids and solvation/hydration parameters of drug molecules.<sup>13</sup> Thermodynamic functions of molecular crystals are, in turn, directly dependent on their crystal structure. Attempts to find out the correlation between the crystal structure of compounds and their thermodynamic parameters still remain a hot topic in drug/material design.

This work is a continuation of our previous study of phenyl derivatives of 1,2,4-thiadiazole with different substitution groups.<sup>14,15</sup> The structural formulas of the compounds studied are presented in Figure 1. In this paper, we would like to focus on the detailed description of the crystal structures of the thiadiazole derivatives synthesized so far. In addition, we examine the conformational flexibility of the molecules, the thermophysical properties, and the sublimation thermodynamics in order to find out the relationship between these parameters and the crystal structure.

## 2. EXPERIMENTAL METHODS

**2.1. Compounds Synthesis.** The synthesis of 1-[5-amino-1,2,4-thiadiazol-3-yl]propan-2-ols was based on the method of Vivona et al.<sup>16</sup> and described by us earlier.<sup>14,15</sup> 1-[5-Amino-1,2,4-thiadiazol-3-yl]propan-2-ols (4) were prepared by a reduction of appropriated 1-[5-amino-1,2,4-thiadiazol-3-yl]-propan-2-ones (3) (Scheme 1). 1-[5-Amino-1,2,4-thiadiazol-3-yl]propan-2-one (0.01 M) was dissolved in 20 mL of methanol. NaBH<sub>4</sub> (0.015 M) was added portionwise to the solution, and the mixture was stirred for 30 min, at the same time hydrogen gassing was stopped. The solvent was removed until the resultant residue was dry, and then the residue was taken up in dichloromethane/water. The organic layer was separated, dried

over Na<sub>2</sub>SO<sub>4</sub>, and filtered. The solvent was evaporated. The crude powder was recrystallized from isopropanol to derive the final product. The synthetic method for ketones (3) is based on Boulton-Katritzky's rearrangement<sup>17</sup> of isoxazolic thiourea (2) (obtained by a standard reaction between isothiocyanates and 3-amino-5-methyl-isoxazole (1) in dipolar aprotic solvents (DMSO, acetonitrile) to 1,2,4-thiadiazoles). At room temperature, the reaction in DMSO passes completely in 5–6 h.<sup>18</sup> All solvents were of AR grade.

**2.2. Single Crystal Preparation.** Single crystals of the compounds were grown by slow evaporation of solvent from methanol/water solutions (20:1).

**2.3. X-ray Diffraction Experiments.** Single-crystal X-ray measurements were carried out using a Nonius CAD-4 diffractometer with graphite-monochromated Mo K $\alpha$  radiation ( $\lambda = 0.71069 \text{ \AA}$ ). The intensity data were collected at 25 °C by means of a  $\omega$ -2 $\theta$  scanning procedure. The crystal structures were solved by direct methods and refined through a full-matrix least-squares procedure. CAD-4 software<sup>19</sup> was applied for data collection, data reduction, and cell refinement. SHELXS-97 and SHELXL-97 programs<sup>20</sup> were used to solve and to refine structures, respectively.

**2.4. Sublimation Experiments.** Sublimation experiments were carried out by the transpiration method described elsewhere.<sup>21</sup> In brief, a stream of an inert gas passes above the sample at the predetermined slow constant flow rate under a constant temperature in order to saturate the carrier gas with the vapor of the tested substance. The vapor condenses at some point downstream and the sublimate mass as well as its purity is determined. The vapor pressure over the sample at this temperature can be calculated based on the amount of the sublimated sample and the volume of the inert gas used.

The equipment was calibrated using benzoic acid. The standard value of sublimation enthalpy obtained here was  $\Delta H_{\text{sub}}^0 = 90.5 \pm 0.3 \text{ J}\cdot\text{mol}^{-1}$ . This is in good agreement with the value recommended by IUPAC of  $\Delta H_{\text{sub}}^0 = 89.7 \pm 0.5 \text{ J}\cdot\text{mol}^{-1}$ .<sup>22</sup> The saturated vapor pressures were measured at each temperature five times with the standard deviation being within 3–5%. Since the saturated vapor pressure of the tested compounds is low, it may be assumed that the heat capacity change of the vapor with temperature is negligible. The experimentally determined vapor pressure data may be described in  $(\ln P; 1/T)$  coordinates in the following way:

Scheme 1. Reaction Scheme for Preparing Novel 1,2,4-Thiadiazoles

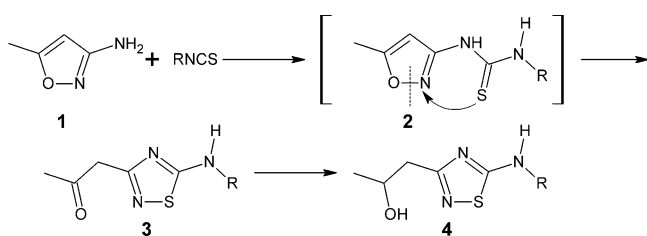


Table 1. Selected Crystallographic Data for Compounds VII–XII

	VII	VIII	IX	X	XI	XII	compd reference
chemical formula	C <sub>12</sub> H <sub>15</sub> N <sub>3</sub> O <sub>2</sub> S	C <sub>12</sub> H <sub>14</sub> ClN <sub>3</sub> OS	C <sub>11</sub> H <sub>12</sub> ClN <sub>3</sub> OS	C <sub>12</sub> H <sub>15</sub> N <sub>3</sub> O <sub>1</sub> S <sub>1</sub>	C <sub>11</sub> H <sub>12</sub> Cl <sub>1</sub> N <sub>3</sub> O <sub>1</sub> S <sub>1</sub>	C <sub>12</sub> H <sub>14</sub> Cl <sub>1</sub> N <sub>3</sub> O <sub>1</sub> S <sub>1</sub>	
formula mass	265.33	283.77	269.75	249.34	269.75	283.78	
crystal system	monoclinic	triclinic	monoclinic	orthorhombic	monoclinic	orthorhombic	
a/Å	11.299(3)	7.515(3)	8.7382(14)	8.6335(2)	12.606(8)	9.4374(3)	
b/Å	7.254(2)	12.070(5)	11.7601(18)	14.1307(3)	12.807(8)	13.0463(4)	
c/Å	15.444(5)	15.831(7)	11.8741(19)	21.2871(5)	7.633(7)	22.2127(6)	
α/deg	90.00	70.379(7)	90.00	90.00	90.00	90.00	
β/deg	101.681(5)	78.224(7)	99.503(2)	90.00	90.590(3)	90.00	
γ/deg	90.00	74.463(7)	90.00	90.00	90.00	90.00	
unit cell volume/Å <sup>3</sup>	1239.7(6)	1292.8(10)	1203.5(3)	2596.97(10)	1232.2(16)	2734.90(14)	
T/K	173(2)	173(2)	173(2)	293(2)	293(2)	293(2)	
space group	P21/c	P – 1	P21/c	Pbca	P21/c	Pbca	
no. of formula units per unit cell, Z	4	4	4	8	4	8	
no. of reflections measured	9627	10 107	11 255	66 101	15 882	58 981	
no. of independent reflections	2701	4984	2623	3643	2309	3118	
R <sub>int</sub>	0.0429	0.0343	0.0257	0.028	0.052	0.031	
final R <sub>1</sub> values (I > 2σ(I))	0.0374	0.0521	0.0316	0.0527	0.0536	0.0491	
final wR(F <sup>2</sup> ) values (I > 2σ(I))	0.0923	0.1277	0.0785	0.0505	0.0511	0.0531	
final R <sub>1</sub> values (all data)	0.0516	0.0816	0.0393	0.0450	0.0679	0.0548	
final wR(F <sup>2</sup> ) values (all data)	0.0993	0.1455	0.0820	0.0455	0.0484	0.0511	
goodness of fit on F <sup>2</sup>	1.033	1.035	1.048	1.0748	1.1221	1.0895	

$$\ln P = A + \frac{B}{T} \quad (1)$$

The value of the sublimation enthalpy is calculated by the Clausius–Clapeyron equation:

$$\Delta H_{\text{sub}}^T = RT^2 \frac{\partial(\ln P)}{\partial T} \quad (2)$$

whereas the sublimation entropy at a given temperature *T* was calculated by the following relation:

$$\Delta S_{\text{sub}}^T = \frac{(\Delta H_{\text{sub}}^T - \Delta G_{\text{sub}}^T)}{T} \quad (3)$$

with  $\Delta G_{\text{sub}}^T = -RT \ln(P/P_0)$ , where  $P_0 = 10^5$  Pa.

For experimental reasons, the sublimation data are given at elevated temperatures. However, in comparison with effusion methods, the temperatures in our case are much lower which makes the extrapolation to room temperature conditions easier. In order to further improve the extrapolation to room conditions, heat capacities ( $C_{p,\text{cr}}^{298}$ -value) of the crystals were estimated using the additive scheme proposed by Chickos and Acree.<sup>23</sup> Heat capacity was introduced as a correction for the recalculation of the sublimation enthalpy  $\Delta H_{\text{sub}}^T$ -value at 298 K ( $\Delta H_{\text{sub}}^0$ -value) according to the equation:<sup>23</sup>

$$\begin{aligned} \Delta H_{\text{sub}}^0 &= \Delta H_{\text{sub}}^T + \Delta H_{\text{cor}} \\ &= \Delta H_{\text{sub}}^T + (0.75 + 0.15C_{p,\text{cr}}^{298})(T - 298.15) \end{aligned} \quad (4)$$

**2.5. Differential Scanning Calorimetry.** Differential scanning calorimetry (DSC) was carried out using a DSC 204 F1 “Phoenix” (Netzsch, Germany) instrument. DSC runs were performed in an atmosphere of flowing (25 mL·min<sup>−1</sup>) dry argon gas of high purity 99.996% using standard aluminum sample pans and a heating rate of 10 K·min<sup>−1</sup>. The DSC instrument was calibrated using five standards: Hg, biphenyl, indium, tin, and bismuth. The sample mass was determined with an accuracy of  $1 \times 10^{-5}$  g using the balance Sartorius M2P.

**2.6. Calculation Procedure.** The free molecular volume in the crystal lattice was estimated on the basis of the X-ray diffraction data and van der Waals molecular volume ( $V_{\text{vdw}}$ ) calculated using the spatial descriptors in Materials Studio. For the disordered structures  $V_{\text{vdw}}$ -values have been calculated for the coordinates of atoms with maximal probability. Molecular free volume ( $V_{\text{free}}$ ) has been evaluated as

$$V_{\text{free}} = \frac{(V_{\text{cell}} - ZV_{\text{vdw}})}{Z} \quad (5)$$

where  $V_{\text{cell}}$  is the volume of the unit cell and  $Z$  is the number of molecules in the unit cell. In order to describe the molecules packing density changes in the crystals, the parameter  $\beta = V_{\text{free}}/V_{\text{vdw}}$  has been introduced earlier.<sup>24</sup> It shows the change of the free volume falling on one molecule in the crystal, with increasing of it is van der Waals volume.

Geometry optimization and single point quantum mechanical calculations were carried out in Accelrys Materials Studio by using the density functional program DMol3 at BLYP/GGA<sup>25–29</sup> level of theory, and DNP basis set. Since no imaginary frequency was found, all the optimized structures were characterized as minima. All torsion profile calculations were performed using the scan step of 10°. The fully optimized thiadiazol molecule was used as a starting point.

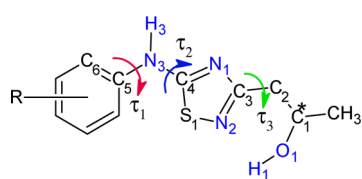
### 3. RESULTS AND DISCUSSION

**3.1. Crystal Structure Analysis. Conformation Analysis.** Structures I–VI have been briefly described in our previous papers,<sup>14,15</sup> while VII–XII are new compounds. The results of the X-ray diffraction experiments are summarized in Table 1.

The conformational state of the thiadiazole molecules under study can be described in terms of three torsion angles  $\tau_1$ ,  $\tau_2$ , and  $\tau_3$ , which are shown in Scheme 2.

The values of  $\tau_1$ ,  $\tau_2$ , and  $\tau_3$  angles (for identical enantiomers) are reported in Table 2. The torsion angles  $\tau_1$  and  $\tau_2$  are responsible for the location of the phenyl and the thiadiazole rings, respectively. While the torsion angle  $\tau_3$  characterizes the

**Scheme 2. Donor and Acceptor Atoms Involved in Hydrogen Bond Formation (colored in blue)<sup>a</sup>**



<sup>a</sup>The asterisk marks the chiral center of the molecule. Flexible torsion angles are indicated by  $\tau_1$ ,  $\tau_2$ , and  $\tau_3$ .

flexibility of the alcohol group. In addition, we introduced an angle between the phenyl and the thiadiazole rings referenced here after as  $\alpha$  (the acute angle between the least-squares planes through the two rings) (Table 2).

One can notice that  $\tau_1$  is generally located around  $180^\circ$ . There are a few exceptions though; namely, compounds V, VIII, and XI have  $\tau_1$  values around  $140^\circ$ . For the majority of molecules, the torsion angle  $\tau_2$  is fixed near  $0^\circ$ . However, molecules IX, X, and XII adopt the second possible thiadiazole ring configuration, wherein  $\tau_2$  is located at about  $-180^\circ$ . This kind of conformation is inverse compared to the first one. It should be noted that significant differences in the thiadiazole ring orientation have only a minor effect on the angle between the phenyl and the thiadiazole rings ( $\alpha$ ). As a result, molecules remain relatively flat which corresponds to an energy minimum state (this problem will be discussed below). The main conformational differences between molecules (apart from thiadiazole ring rotation) are concentrated in the alcohol fragment. Table 2 shows that the  $\tau_3$  angle changes within a rather broad range: from  $124.8^\circ$  to  $-113.3^\circ$ . There is no doubt that such diversity of  $\tau_3$  values is provided by high flexibility of the alcohol group due to the low conformational energy barrier.

Ultimately, all structures can be conventionally divided into three groups based on distribution of the torsion angles  $\tau_1$ ,  $\tau_2$ , and  $\tau_3$ . The first group includes compounds I, II, III, and XI. In this group, rotation along the  $\tau_3$  angle is restricted by the intramolecular hydrogen bond O1–H1…N1;  $\tau_2$  values are located in the low angle region. The second group consists of the following compounds: IV, V, VI, VII, and VIII. These molecules are characterized by a large variation of the  $\tau_1$  and  $\tau_3$  torsion angles values, while the  $\tau_2$  angle does not change significantly. The third group covers the “inverse” molecules IX, X, and XII. The torsion angles  $\tau_1$  and  $\tau_2$  in this case are fixed at

high angle values. However, the  $\tau_3$  is free to vary within a  $20^\circ$  range.

It is evident that the conformational state of each molecule in a crystal results from the effect of two factors: packing forces (van der Waals interactions, hydrogen bonds, etc.) and conformation energy. Therefore, it would be interesting to analyze the hydrogen bond patterns and the crystal structure features of the compounds belonging to different conformational groups.

**Hydrogen Bonds and Packing Architecture Analysis.** Hydrogen bonds play an essential role in the crystal structures of the studied molecules. Moreover, the number of hydrogen bonds per molecule varies from one to three creating rather different network topologies. The most convenient way to describe and classify H-bonds is to apply the graph set notation terminology introduced by Etter<sup>30</sup> and revised by Bernstein.<sup>31</sup> The comparative characteristics of the hydrogen bond geometric parameters, graph set assignments are summarized in Table 3. The illustrations of the individual H-bond motifs of the first level are shown in Figure 2 (Illustrations of the second level of graph set assignments matrix are shown in the Supporting Information).

If the diagonal elements of the graph set assignments matrix (the first level) are considered, the graph set notation C(8) is the most frequent H-bond motif in the studied structures. It appears nine times, whereas R<sub>2</sub><sup>2</sup>(16), R<sub>2</sub><sup>2</sup>(12), and C(6) graph sets are observed only three times each. Moreover, the dimer arrangement is more typical of O1–H1…N1(2) bonds, while N3–H3…O1 H-bonds usually form ribbons.

Since the crystal lattice of all the compounds contains two cocrystallized enantiomers (racemic crystal), we tried to trace the hydrogen bond arrangement in different enantiomer pairs. Figure 2 shows the combination of such pairs generated along the hydrogen bonds, where S corresponds to the left-hand enantiomer and R corresponds to the right-hand enantiomer. It is evident that the ribbonlike structures (graph set notation C(8), C(6)) contain molecules of one enantiomer only, while the rings (graph set notations R<sub>2</sub><sup>2</sup>(16), R<sub>2</sub><sup>2</sup>(12)) are formed by molecules of the opposite chirality. However, in compound IV, the S–R enantiomer pairs create both ribbon and ring structures, whereas the homochiral molecules are not connected by hydrogen bonds directly.

All the molecules have been previously divided into three conformational groups based on the distribution of the torsion angles  $\tau_1$ ,  $\tau_2$ , and  $\tau_3$ . It is evident, that the molecules with the

**Table 2. Selected Torsion Angles and Angles between the Phenyl and the Thiadiazole Planes of the Thiadiazole Molecules in the Crystal Structures**

substance	$\tau_1(C_4-N_3-C_5-C_6)$ , deg	$\tau_2(S_1-C_4-N_3-C_5)$ , deg	$\tau_3(C_1-C_2-C_3-N_2)$ , deg	$\alpha$ , deg
I	-173.0	2.6	131.8	9.4
II	-174.0	3.4	145.8	9.9
III	179.0	-0.6	154.6	1.4
IV	174.4	3.5	-105.7	5.5
V	136.8	-3.7	36.8	47.2
VI	163.3	13.5	-107.6	16.6
VII	-171.3	2.4	-8.6	11.1
VIII	141.2	-5.6	42.4	43.6
IX	-170.9	-175.4	-133.4	14.5
X	174.1	-169.0	-122.3	3.7
XI	144.6	-1.3	124.8	36.9
XII	-174.6	-173.8	-113.3	8.0

Table 3. Hydrogen Bond Geometry, Graph Set of the Compounds Studied

	D—H···A <sup>a</sup>	D—H /Å	H···A /Å	D···A /Å	D—H···A /deg	a	b	c	d	
I										
a	N3—H3···O1 <sup>b</sup>	0.864(1)	1.982(1)	2.843(1)	175.1(2)	a	C(8)			
II										
a	N3—H3···O1 <sup>c</sup>	0.860(1)	2.042(1)	2.897(1)	173.2(2)	a	C(8)			
III										
a	N3—H3···O1 <sup>d</sup>	0.847(1)	2.023(1)	2.869(1)	176.3(2)	a	C(8)			
IV										
a	N3—H3···O1 <sup>e</sup>	0.860(3)	1.971(1)	2.811(1)	165.0(1)	a	C(8)			
b	O1—H1···N2 <sup>f</sup>	0.820(8)	1.976(1)	2.786(1)	171.9(2)	b	C <sub>2</sub> <sup>2</sup> (7)	R <sub>2</sub> <sup>2</sup> (12)		
V										
a	N3—H3···O1 <sup>g</sup>	0.860(1)	2.142(6)	2.881(4)	143.7(4)	a	C(8)			
VI										
a	N3—H3···O2 <sup>g</sup>	0.859(1)	2.016(7)	2.867(6)	170.5(3)	a	C(8)			
b	O2—H2···O1 <sup>h</sup>	0.819(6)	1.909(2)	2.720(2)	170.1(3)	b	C <sub>2</sub> <sup>2</sup> (10)	C(14)		
c	O1—H1···N2 <sup>i</sup>	0.819(7)	2.076(8)	2.825(1)	151.6(3)	c	R <sub>4</sub> <sup>4</sup> (38)	R <sub>4</sub> <sup>4</sup> (26)	R <sub>2</sub> <sup>2</sup> (12)	
VII										
a	N3—H3···O1 <sup>j</sup>	0.870(2)	2.020(2)	2.873(2)	170.9(2)	a	C(8)			
VIII										
a	O1—H1···N4 <sup>k</sup>	0.897(3)	1.983(3)	2.878(3)	175.8(3)	a	D(2)			
b	N3—H3···O1 <sup>l</sup>	0.812(3)	2.022(3)	2.827(3)	171.1(3)	b	D <sub>3</sub> <sup>3</sup> (13)	C(8)		
c	O2—H2···N1 <sup>m</sup>	0.843(4)	2.047(4)	2.863(3)	162.8(4)	c	R <sub>2</sub> <sup>2</sup> (12)	D <sub>3</sub> <sup>3</sup> (11)	D(2)	
d	N6—H6···O2 <sup>n</sup>	0.877(3)	1.962(3)	2.822(3)	166.3(3)	d	D <sub>3</sub> <sup>3</sup> (11)	—	D <sub>3</sub> <sup>3</sup> (13)	C(8)
IX										
a	N3—H3···O1 <sup>o</sup>	0.838(2)	1.991(2)	2.827(2)	175.3(2)	a	R <sub>2</sub> <sup>2</sup> (16)			
b	O1—H1···N2 <sup>p</sup>	0.803(2)	2.140(2)	2.933(2)	172.4(2)	b	C <sub>2</sub> <sup>2</sup> (7)	C(6)		
X										
a	N3—H3···O1 <sup>q</sup>	0.902(1)	1.971(1)	2.865(1)	170.5(8)	a	C(8)			
b	O1—H1···N2 <sup>r</sup>	0.881(1)	2.007(1)	2.867(1)	164.9(8)	b	C <sub>2</sub> <sup>2</sup> (7)	C(6)		
XI										
a	N3—H3···O1 <sup>s</sup>	0.886(2)	1.992(2)	2.868(4)	169.6(2)	a	R <sub>2</sub> <sup>2</sup> (16)			
XII										
a	N3—H3···O1 <sup>f</sup>	0.888(1)	2.154(1)	2.993(1)	157.3(1)	a	R <sub>2</sub> <sup>2</sup> (16)			
b	O1—H1···N2 <sup>t</sup>	0.842(2)	2.044(2)	2.882(2)	173.5(1)	b	C <sub>2</sub> <sup>2</sup> (7)	C(6)		

<sup>a</sup>Numbering corresponds to Figure 2. Symmetry codes for acceptor atoms are as follows (*b*—*t*). <sup>b</sup>(−*x*, *y* + 1/2, −*z* + 1/2). <sup>c</sup>(−*x* + 1/2, *y* + 1/2, −*z* + 1/2). <sup>d</sup>(−*x* − 2, *y* + 1/2, −*z* − 1). <sup>e</sup>(−*x* + 1.5, *y* − 1/2, *z*). <sup>f</sup>(−*x* + 1, −*y* + 1, −*z* + 1). <sup>g</sup>(*x* + 1, *y*, *z*). <sup>h</sup>(*x* − 1, *y* + 1, *z*). <sup>i</sup>(−*x*, −*y* + 1, −*z*). <sup>j</sup>(−*x* + 1, *y* + 1/2, −*z* + 1/2). <sup>k</sup>(*x*, *y* − 1, *z*). <sup>l</sup>(*x* + 1, *y*, *z*). <sup>m</sup>(*x*, *y* + 1, *z*). <sup>n</sup>(*x* − 1, *y*, *z*). <sup>o</sup>(−*x* + 2, −*y* + 1, −*z*). <sup>p</sup>(−*x* + 2, *y* − 1/2, −*z* − 1/2). <sup>q</sup>(−*x* + 2, *y* − 1/2, *z* − 1.5). <sup>r</sup>(−*x* + 1/2, *y*, −*z* + 1.5). <sup>s</sup>(−*x* + 1, −*y*, −*z* + 1). <sup>t</sup>(*x* + 1/2, −*y* + 1.5, −*z* + 1).

conformation restricted by the intramolecular hydrogen bond O1—H1···N1 (the first group) are not able to form a complex H-bond network. It would be reasonable to assume that the van der Waals forces most significantly contribute to the lattice energy in this case. In fact, the packing of I, II, and III is very similar. It can be described as perpendicular side-to-side stacks of the molecules joined together by H-bonds and interacting via van der Waals force inside of each stack. As a result, a herringbone structure is formed (Figure 3).

In contrast to I, II, and III, the crystal of XI consists of the centrosymmetric H-bond dimers of the molecules arranged as the parallel columns (Figure 4).

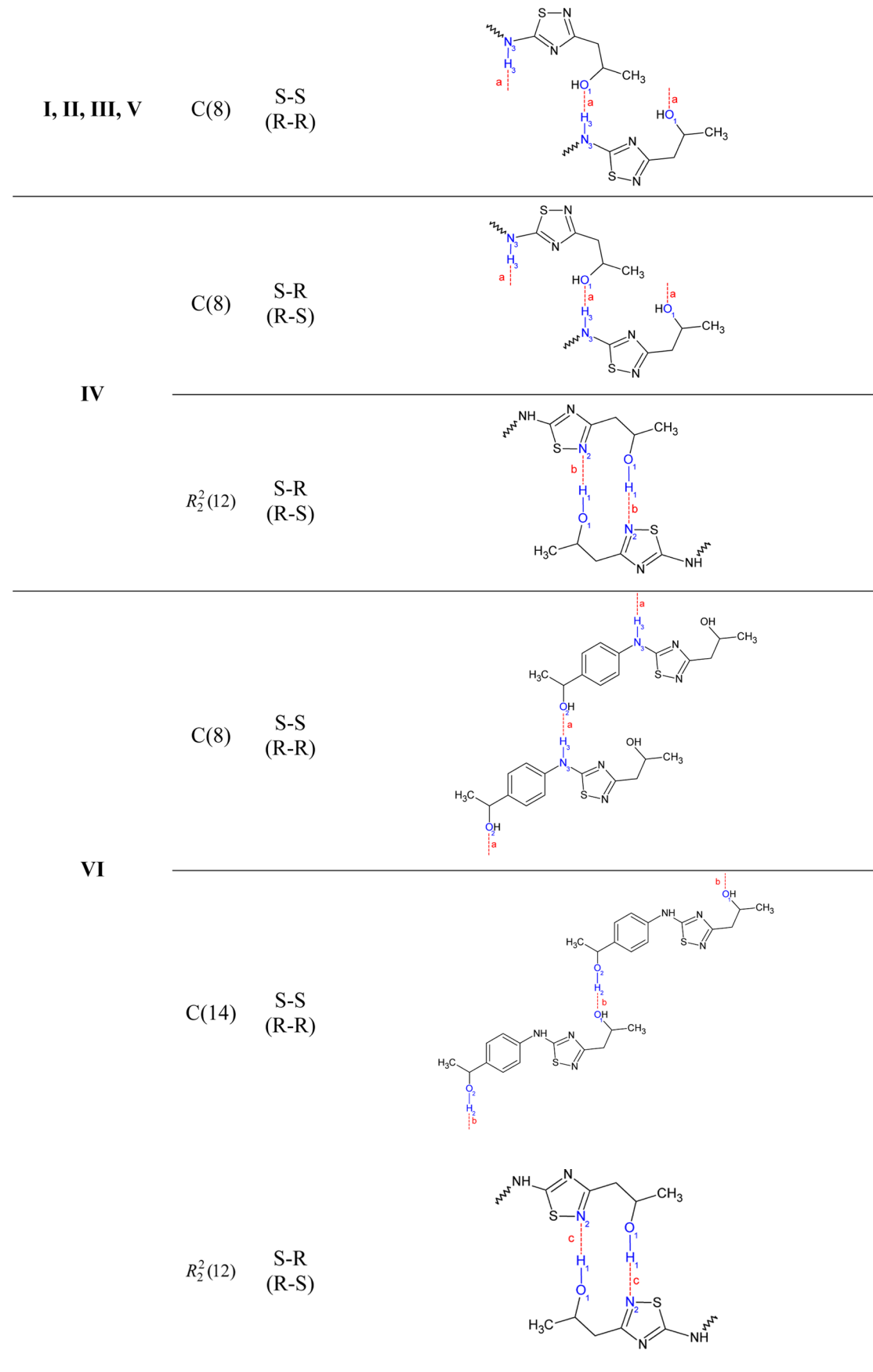
The second group of compounds (IV, V, VI, VII, and VIII) shows diversity of packing architecture. The crystal of VII is constructed from chains of the homochiral molecules joined by H-bonds along the *b*-axes, whereas the neighboring chains interact through van der Waals forces (Figure 5). We believe that this packing structure is in a way the consequence of the alcohol group rotation about the  $\tau_3$  angle.

Crystals IV and V consist of zigzag layers connected with each other by one (V) or two (IV) hydrogen bonds. The distances between crests within the zigzag chain are about 18.2

Å for V and 23.2 Å for IV (Figure 6). Interestingly, the ratio of the mentioned distances (23.2/18.2 = 1.27) is quite close to that of the packing density parameters  $\beta$ : 56.2%/45.7% = 1.23 (Table 4).

The asymmetric unit of VIII contains two molecules of opposite chirality. The crystal of VIII is constructed from distinct layers of symmetry unequivalent molecules (Figure 7). The neighbor layers are assembled into a 3D structure in the crystal via van der Waals interactions between the phenyl and/or the thiadiazole fragments. In addition, the phenyl–phenyl interactions occur between A and B molecules only, while the thiadiazole fragments are responsible for A–A and B–B close contacts.

The crystal structure of VI is unique among the others because of its additional site of hydrogen bonding. As Table 3 shows, the diagonal elements of the graph set assignments matrix for VI consist of two infinite chains and one dimer. Two chains, C(8) and C(14), translate the molecules along *a* and *b* directions, respectively. The chains of molecules of the opposite chirality combine with each other via the ring motive (R<sub>2</sub><sup>2</sup>(12)) to form a complicated 3D sheets. So the overall structure

**Figure 2.** continued

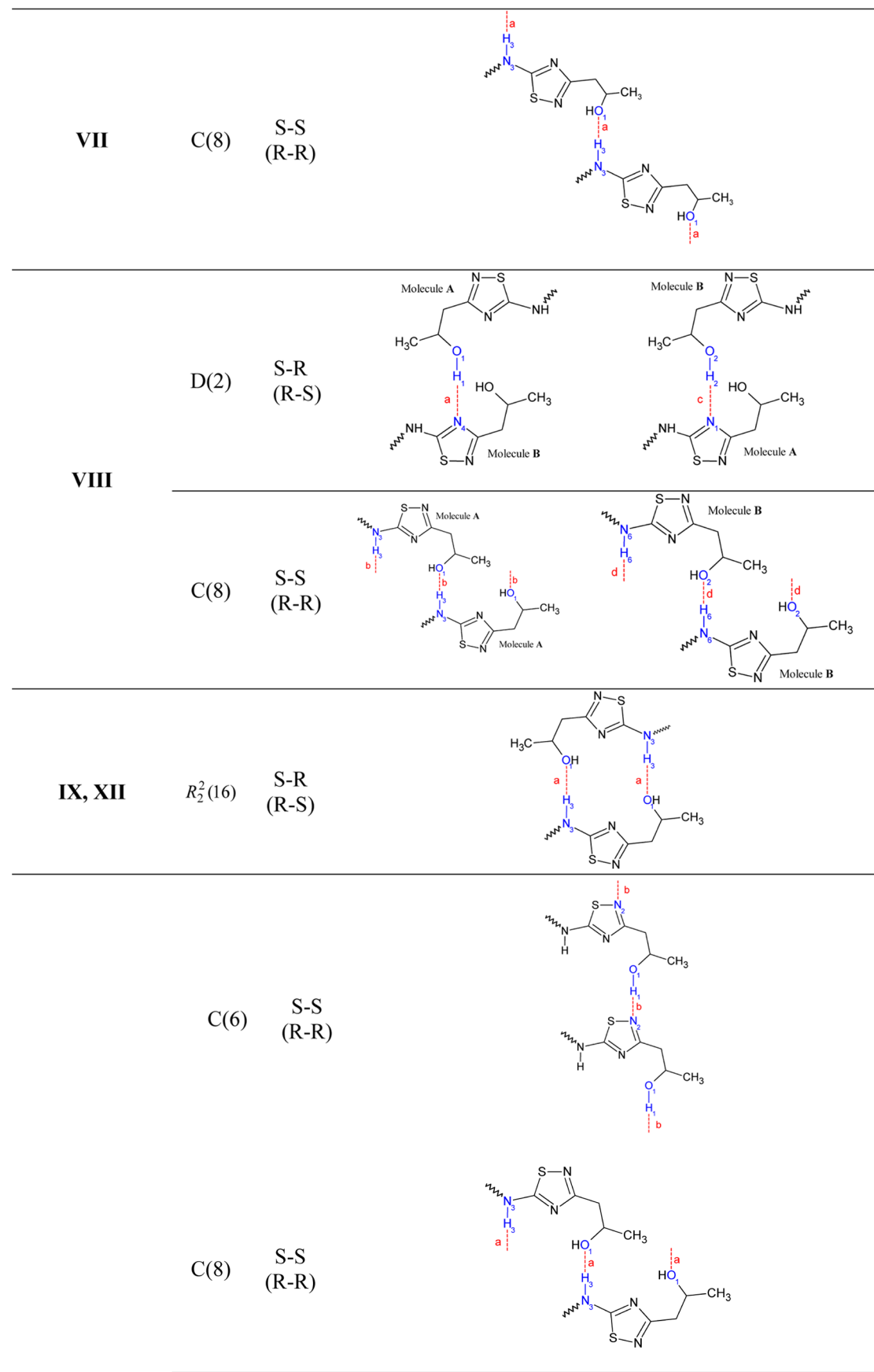


Figure 2. continued

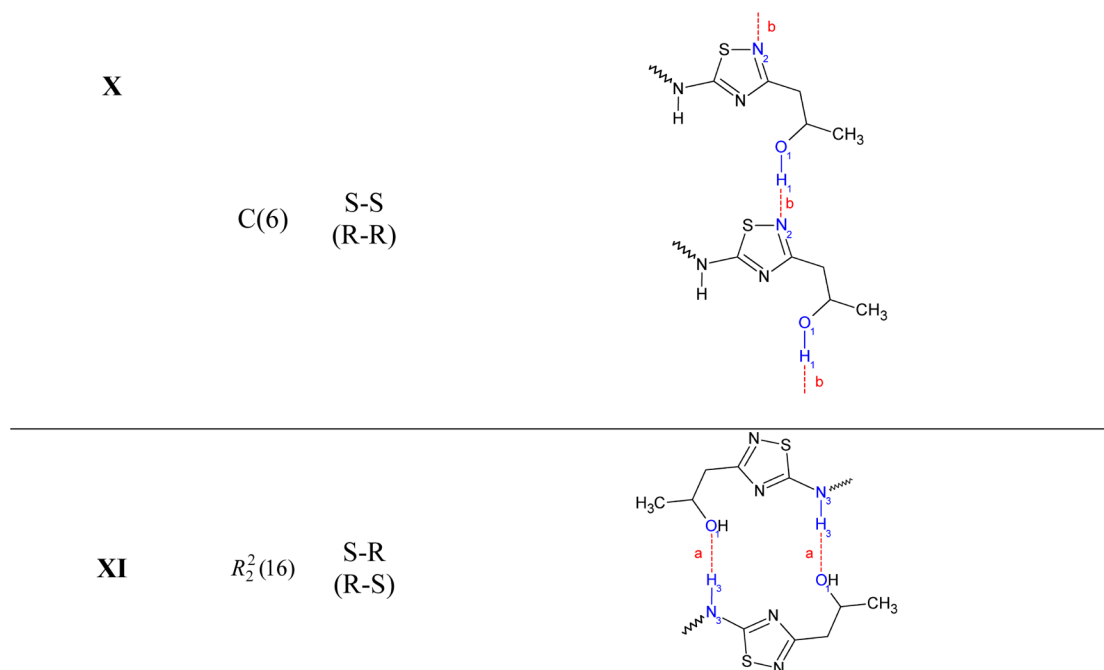


Figure 2. Illustrations of the individual H-bond motives occurring in crystals of the compounds studied (first level).

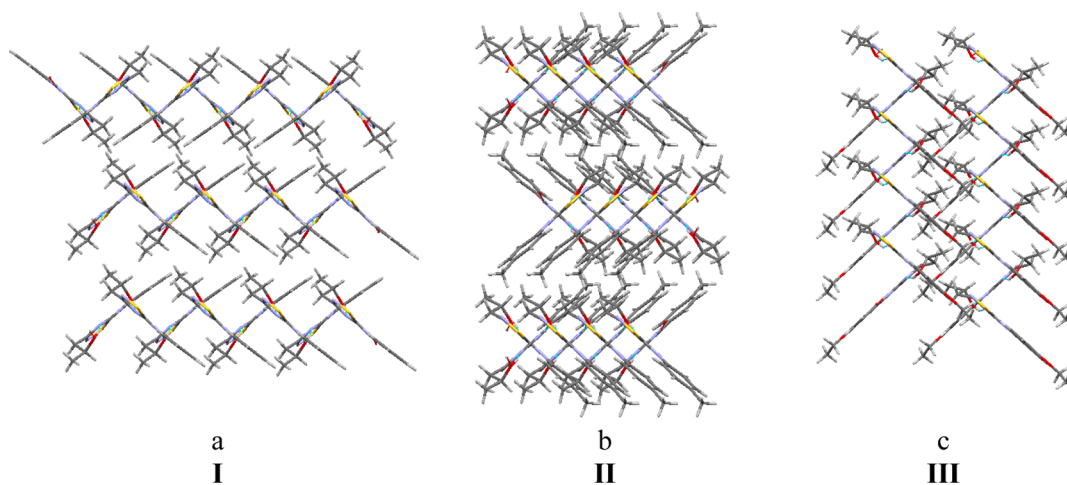


Figure 3. Molecular packing projections for the compounds with herringbone structure.

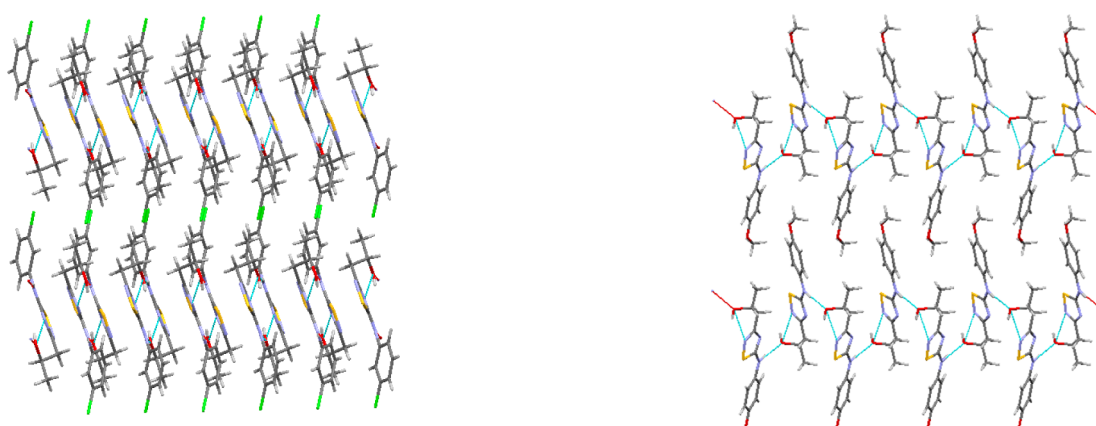


Figure 4. Projections of molecular packing for XI along the *b*-axis with dimer organization of crystal structure.

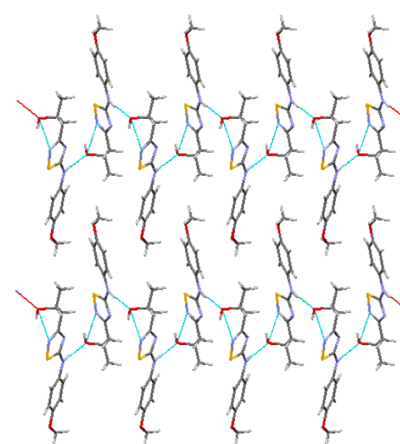
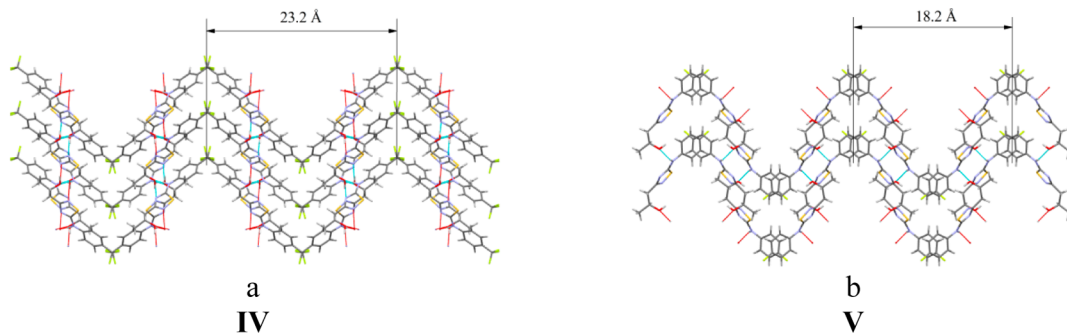


Figure 5. View of molecular chain organization in the crystal structure of VII along the *a*-axis.

Figure 6. Packing projections of IV (along the *a*-axis) and V (along the *c*-axis).**Table 4.** van der Waals Volumes,  $V_{\text{vdw}}$ , Molecular Free Volumes,  $V_{\text{free}}$ , and Packing Density Parameter,  $\beta$ , for the Compounds Studied

substance	$V_{\text{vdw}}$ Å <sup>3</sup>	$V_{\text{free}}$ Å <sup>3</sup>	$V_{\text{free}}/V_{\text{vdw}} (\beta)$ %
I	197.0	89.2	45.3
II	213.1	93.9	44.1
III	237.7	107.6	45.3
IV	227.8	128.1	56.2
V	202.3	92.5	45.7
VI	236.4	115.6	48.9
VII	222.0	87.9	39.6
VIII	228.6	94.6	41.4
IX	213.4	87.5	41.0
X	216.3	108.3	50.1
XI	211.8	96.3	45.5
XII	229.8	112.1	48.8

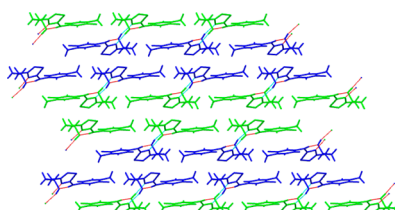


Figure 7. Molecular packing projections for VIII. Asymmetric molecules are colored in blue and green for clarity.

consists of such sheets interacting by means of van der Waals forces (Figure 8).

The packing structures of the third group of the molecules (IX, X, and XII) are quite similar in contrast to those of the second group. All the crystals are built from distinct layers of the hydrogen bonded molecules running along the *a*-axis (X and XII) or *b*-axis (IX) (Figure 9). As a result, the neighbor

layers interact through the weak van der Waals forces between the phenyl fragments. However, the molecules are tightly held via 2D network of H-bonds inside the layer.

It is evident that all the crystals described above can be arranged according to the ratio of their hydrogen bonds to van der Waals forces. In the first group of compounds, the van der Waals forces are clearly dominant over H-bond energies. In the third group, the ratio is shifted to the hydrogen bonds, which are responsible for layer construction. The crystal structures of the second group compounds show a broad spectrum in the ratio of H-bonds to van der Waals forces. In fact, the crystals of VII and V are mainly stabilized by the van der Waals interaction. In case of IV and VI, H-bonds occupy a significant part of intralayer space, while the molecules belonging to the layers are assembled into a crystal via van der Waals interactions. In the crystal of VI, the network of H-bonds covers almost all the structure, so the van der Waals forces play a role in the interlayer space only.

**3.2. Computational Study.** In order to investigate conformational preferences of the molecules outside of the crystal environment, conformational scans of torsion angles  $\tau_1$ ,  $\tau_2$ , and  $\tau_3$  were constructed at the BLYP/DNP level of theory in Materials Studio using the scan step of  $10^\circ$  allowing the rest of the molecule to relax. As a starting point, each thiadiazole molecule was fully optimized on the same level of theory. The geometrical parameters of the thiadiazole molecules after the optimization are shown in Table 5.

It turns out that the relative position of the H1 atom and thiadiazole ring has a significant influence on molecular stabilization energy because of intramolecular hydrogen bond formation. Moreover, the H1 atom being fixed by intramolecular hydrogen bond near the steady position is no longer available for intermolecular hydrogen bonding. The position of H1 with respect to N1 can be described in terms of anti–syn

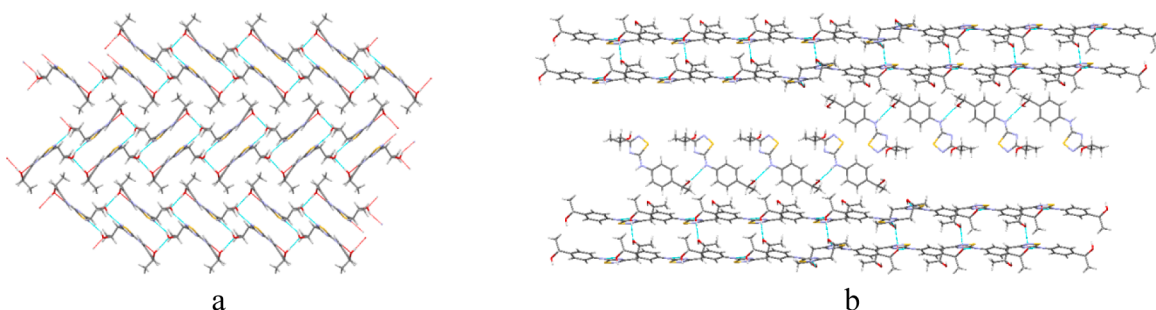
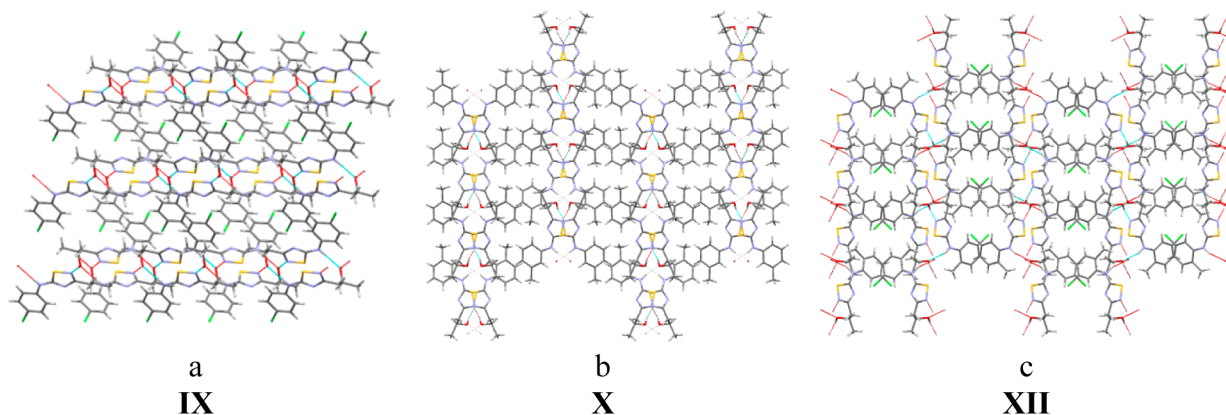


Figure 8. Two projections of molecular packing of VI with ring (a) and chain (b) organization of crystal structure.



**Figure 9.** Packing projection of **IX** (along *c*-axis), **X**, and **XII** (along *a*-axis).

**Table 5. Selected Torsion Angles, Angles between the Phenyl and the Thiadiazole Planes of the Thiadiazole Molecules after Optimization Procedure at the BLYP/GGA/DNP Level of Theory and Conformations of Alcohol Group in the Compounds in Terms of anti–syn Notation (see text)**

substance	$\tau_1$ , deg	$\tau_2$ , deg	$\tau_3$ , deg	$\alpha$ , deg	conformation of alcohol group
I	-172.6	-0.2	131.9	7.7	anti
II	169.1	-1.7	129.9	12.5	anti
III	151.9	-0.1	129.0	29.1	anti
IV	-173.8	-2.7	129.6	5.2	syn
V	178.7	-2.7	-23.9	3.9	anti
VI	169.2	-0.8	129.0	11.6	syn
VII	-158.1	-3.3	-22.5	20.6	anti
VIII	176.2	0.7	-23.1	3.6	syn
IX	-178.4	179.5	20.9	1.6	syn
X	-172.4	176.8	38.3	6.6	syn
XI	171.9	-1.1	129.9	9.0	anti
XII	177.1	-179.5	17.3	2.9	syn

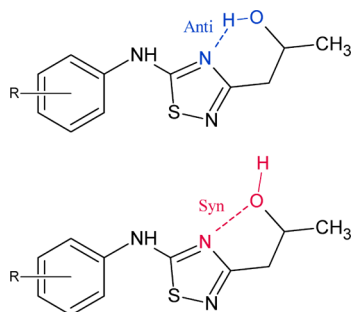


**Figure 10.** Illustration of anti and syn conformation of alcohol group in the compounds studied.

notation (Figure 10). The molecules belonging to anti- and syn-conformations are listed in Table 5.

It is evident that only the syn-conformation of the hydroxy group provides an opportunity for a new intermolecular hydrogen bond to be formed. Meanwhile, this H-bond should be energy-profitable in order to compensate for the conformational destabilization of a molecule (conformational strain), which is caused by the rotation of the alcoholic group about  $\tau_3$  angle. The results of the  $\tau_3$ -constrained optimization of I, II, III, V, VII, and XI (anti-conformation) are shown in Figure 11.

A number of regularities have to be pointed out: (a) all the conformational profiles have an identical shape; (b) the

locations of the energy maxima and minima coincide for all the molecules within several degrees; (c) in all cases, the energy barrier height is relatively low and it does not exceed 14 kJ·mol<sup>-1</sup>. Figure 11 shows that the conformational flexibility of the alcoholic group is slightly influenced by the chemical nature as well as the substituent position in a phenyl ring. Therefore, the  $\tau_3$  value of a molecule in a crystal can be considered a consequence of supramolecular surroundings (ensemble of neighboring molecules) and a function of packing energy. In the case of I, II, III, and XI crystals, the conformational minima of the molecules coincide with the packing energy minimum. However, the crystal formation of V and VII consisting of molecules with the minimum of conformational energy would be impossible or would lead to metastable structures.

Figure 12 shows the results of the  $\tau_3$ -constrained optimization of IV, VI, and VIII molecules (syn-conformation). The conformational profile shapes in this case are rather different as compared to the molecules described above. The calculations reveal that the syn-conformation of OH group is metastable within the whole range of  $\tau_3$ -angle values because of the repulsion between O1 and N1(2) atoms. It is confirmed by the results of the molecule unconstrained optimization that leads to the transition from syn- to anti-conformation. As Figure 12 shows, the stabilization energy produced by intramolecular hydrogen bonding is equal to ca. 24 kJ·mol<sup>-1</sup>. The largest conformational strain of  $\tau_3$ -angle is observed for VIII, while IV and VI are found to be located near a local energy minimum.

It is evident that the anti–syn conformational transitions are a consequence of the competition between two forces: molecule stabilization energy (intramolecular hydrogen bonds) and packing energy (intermolecular hydrogen bonds). This situation is promoted by the high flexibility of the alcohol group, the rotation barrier energy of which is low. The balance is reached when the packing energy gain via the formation of additional H-bonds covers relatively small conformational strains of molecules. It should be noted that it only takes place in the crystals that cannot be constructed from molecules with the minimum conformational energy.

The anti–syn conformational transitions are also observed in the group of “inverse” molecules (IX, X, and XII). The  $\tau_3$ -constrained optimization results are shown in Figure 13. The calculations revealed that the conformational states of all the molecules in a crystal correspond to the local energy minimum. In the case of IX and XII (syn-conformation), the

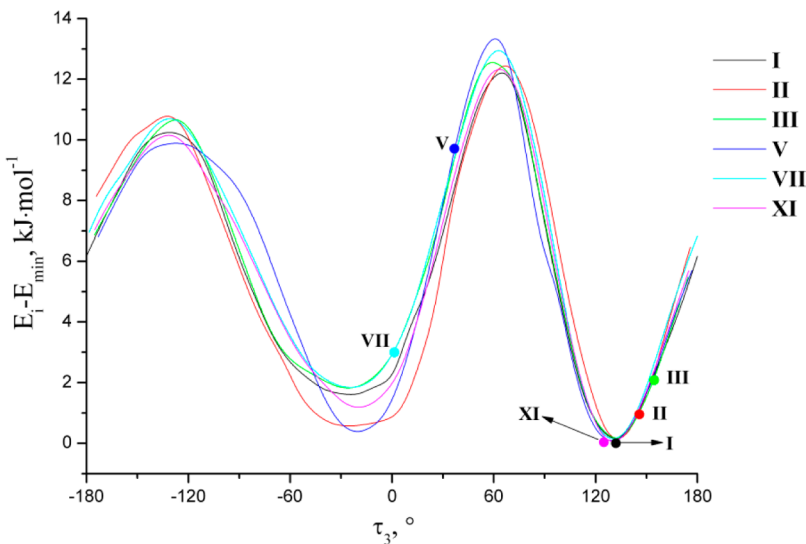


**Figure 11.**  $\tau_3$ -Constrained optimization for molecules with anti-conformation of alcohol group performed at the BLYP/DNP level of theory. The experimental values of  $\tau_3$  in a crystal are marked as the colored dots.

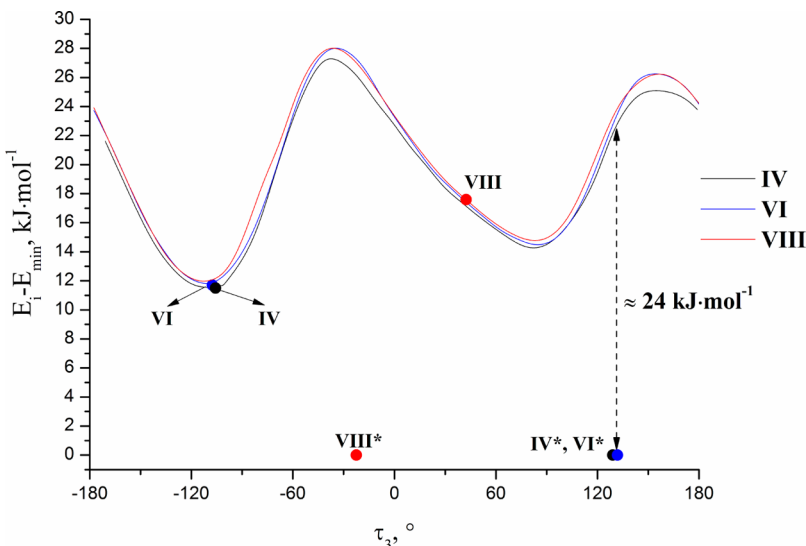


**Figure 12.**  $\tau_3$ -Constrained optimization for molecules with syn-conformation of alcohol group performed at the BLYP/DNP level of theory. The experimental values of  $\tau_3$  in a crystal are marked as colored dots. The values of  $\tau_3$  corresponding to energy minimum are indicated by the asterisk.

destabilization energy of the molecules reaches ca. 10–12 kJ·mol<sup>-1</sup>.

It has to be pointed out that the molecules with the OH group adopting anti-conformation are forced to create hydrogen bond chains in a crystal. In case of XI, the dimeric organization of H-bonds can be correlated to the requirements of special conditions for phenyl fragment packing. On the other hand, the H-bonded dimers are more typical of the molecules with OH group syn-conformation. We believe that the different organization of the H-bonds in a crystal is mainly caused by a deviation of a molecule from the conformation corresponding to the energy minimum (conformational strain). It might be supposed that the stabilization effect due to the formation of the H-bonded dimers would be more significant compared to the chain organization and, in turn, allows greater conformational strains. Consequently, the packing energy of the crystal constructed from the molecules with the minimum conformational energy (anti-conformation) would be minimized by the

van der Waals interactions. While the hydrogen bonds play a secondary role in this process.

The analogous calculations have been performed for the  $\tau_1$  torsion angle from 0° to 180° (Figure 14). One can see that the height and steepness of the energy barrier strongly depend on the substituent nature and its position. However, the shape of the rotation profile remains unchanged in all the studied molecules, i.e. two symmetrical energy minima at 0° and 180°. For XII, the energy profile differs because of the steric hindrance induced by the bulky methyl substituent. Figure 14 shows that at the lower and higher  $\tau_1$ -angle ranges, the rotation energy requirement for the phenyl group is relatively small (except for XII): rotation by 30° requires 1–3 kJ·mol<sup>-1</sup>. Therefore, a wide set of conformations is available for packing during the nucleation and growth of crystal. Relatively large deviations of the  $\tau_1$ -angle from the equilibrium position are only seen in molecules V, VIII, and XI. According to Figure 14, the packing energy gain in this case should be considerably

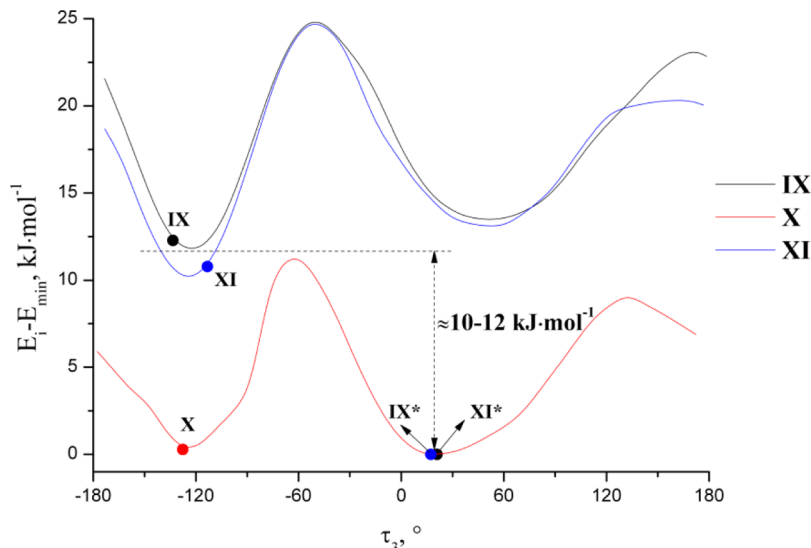


**Figure 13.**  $\tau_3$ -Constrained optimization for “inverse” group of molecules performed at the BLYP/DNP level of theory. The experimental values of  $\tau_3$  in a crystal are marked as colored dots. The values of  $\tau_3$  corresponding to energy minimum are indicated by the asterisk.

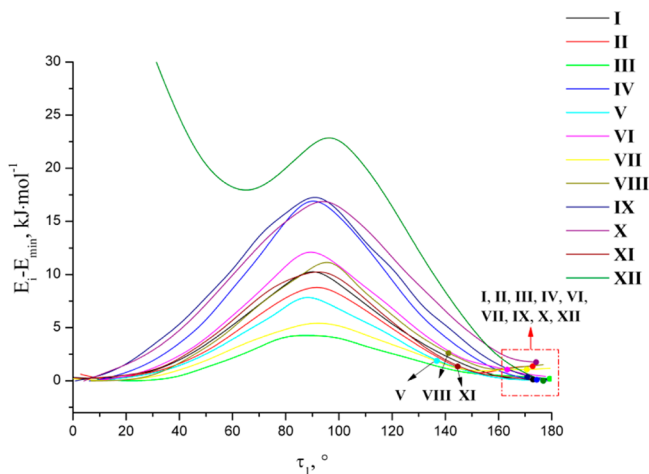


**Figure 14.**  $\tau_1$ -Constrained optimization performed at the BLYP/DNP level of theory. The experimental values of  $\tau_1$  in a crystal are marked as colored dots.

higher than the conformational strains caused by the rotation of the phenyl ring.

The analysis of the  $\tau_2$ -angle distribution of the studied molecules suggests two energy minima for the thiadiazole fragment rotation, namely, at  $0^\circ$  and  $180^\circ$ . The  $\tau_2$ -constrained optimization results are illustrated in Figure 15. It is evident that the  $\tau_2$ -angle energy profile shows a bigger height and steepness as compared to the  $\tau_1$ -angle. It follows that even small deviations of the thiadiazole ring may lead to distinct conformational strains. As a consequence, in the presence of a crystal field, the  $\tau_1$ -angle is allowed to deviate only by  $5\text{--}10^\circ$ , which corresponds to a rather low excess of conformational energy. Molecule VI shows the highest possible  $\tau_1$ -angle value. Probably, it is the additional hydrogen bond in this structure that counterbalances the extra conformational strains.

We concluded that the orientation of different fragments of the thiadiazole molecules in a crystal seems to be defined by the balance between the energy of intermolecular interactions and the energy of conformational strains. The phenyl group rotation requires the least amount of energy, and therefore, it

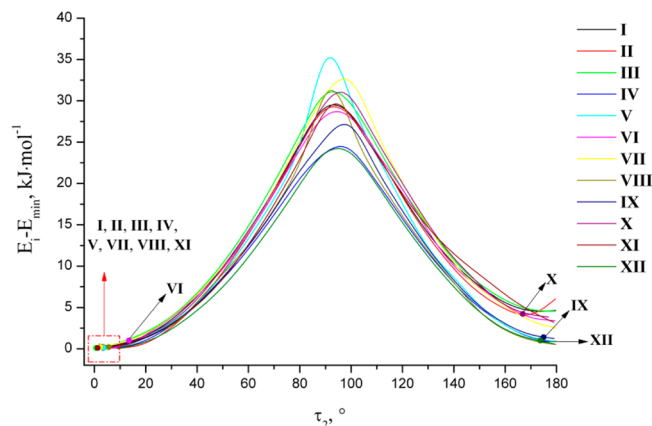


**Figure 15.**  $\tau_2$ -Constrained optimization performed at the BLYP/DNP level of theory. The experimental values of  $\tau_2$  in a crystal are marked as colored dots.

is provided by weak van der Waals forces. However, the new hydrogen bonds need to be formed when the rotation about the  $\tau_2$  and  $\tau_3$  angles is necessary.

### 3.3. Sublimation and Thermophysical Characteristics.

In order to compare the crystal lattice energies and thermochemical characteristics of the compounds under study, sublimation and DSC experiments were carried out. The temperature dependencies of saturated vapor pressure for compounds VII–XII are summarized in Table 6. The thermodynamic functions of sublimation and fusion processes are presented in Table 7. The thermodynamics of sublimation and thermochemical data for I–VI are described in our previous papers.<sup>14,15</sup>

We have tried to calculate crystal lattice energies of the compounds studied using the PIXEL program developed by Gavezzotti.<sup>34</sup> This method provides quantitative determination of crystal lattice energies with a breakdown of these energies to Coulombic ( $E_{\text{coul}}$ ), polarization ( $E_{\text{pol}}$ ), dispersion ( $E_{\text{disp}}$ ), and repulsion ( $E_{\text{rep}}$ ) terms. The theoretical background of the PIXEL approach is based on calculating the electron density of an isolated molecule from the crystal structure molecular geometry using a standard quantum chemical program

Table 6. Temperature Dependencies of Saturation Vapor Pressure of the Compounds Studied

VII <sup>a</sup>		VIII <sup>b</sup>		IX <sup>c</sup>		X <sup>d</sup>		XI <sup>e</sup>		XII <sup>f</sup>	
T [°C]	P × 10 <sup>3</sup> [Pa]	T [°C]	P × 10 <sup>3</sup> [Pa]	T [°C]	P × 10 <sup>3</sup> [Pa]	T [°C]	P × 10 <sup>3</sup> [Pa]	T [°C]	P × 10 <sup>3</sup> [Pa]	T [°C]	P × 10 <sup>3</sup> [Pa]
70.0	1.85	97.0	10.31	88.5	4.31	68.0	2.99	82.0	3.85	74.0	2.44
71.0	1.99	101.0	15.24	89.0	4.87	70.0	3.55	84.0	4.56	76.0	2.84
72.0	2.15	103.0	18.50	91.0	6.10	73.0	5.77	88.0	6.87	78.0	3.43
73.0	2.38	104.0	21.28	103.5	21.67	76.0	7.94	93.0	11.66	80.0	4.01
76.0	4.05	107.0	26.78	106.0	31.62	77.0	9.99	94.5	12.88	82.0	4.94
77.0	4.52	108.0	30.11	108.0	44.29	78.0	10.78	96.0	15.00	84.0	6.04
78.0	5.09	109.0	35.47	110.0	54.97	80.0	14.66	98.0	19.84	85.3	6.65
80.0	5.86	110.0	41.46	111.0	61.95	81.0	16.65	103.0	32.58	90.0	10.03
81.0	7.15	112.0	48.95	113.0	63.74	82.0	19.15	105.0	34.63	92.0	12.91
82.0	8.15	114.0	58.95	115.0	84.33	83.0	20.53	107.0	47.36	93.0	13.76
83.0	8.92	115.0	59.13	116.0	104.09	84.0	23.52			94.0	15.72
		116.0	64.06	118.0	105.40	85.0	26.87				
		118.0	74.72	120.0	124.81	86.0	31.29				
		120.0	91.26								

<sup>a</sup> $\ln(P[\text{Pa}]) = (37.9 \pm 0.7) - (15163 \pm 261)/T; \sigma = 2.7 \times 10^{-2}; r = 0.9993; n = 7.$  <sup>b</sup> $\ln(P[\text{Pa}]) = (33.2 \pm 0.8) - (13989 \pm 317)/T; \sigma = 5.3 \times 10^{-2}; r = 0.9969; n = 14.$  <sup>c</sup> $\ln(P[\text{Pa}]) = (37.5 \pm 0.9) - (15499 \pm 335)/T; \sigma = 9.0 \times 10^{-2}; r = 0.9975; n = 13.$  <sup>d</sup> $\ln(P[\text{Pa}]) = (41.7 \pm 0.7) - (16216 \pm 230)/T; \sigma = 3.7 \times 10^{-2}; r = 0.9989; n = 13.$  <sup>e</sup> $\ln(P[\text{Pa}]) = (32.5 \pm 0.7) - (13513 \pm 251)/T; \sigma = 4.8 \times 10^{-2}; r = 0.9986; n = 10.$  <sup>f</sup> $\ln(P[\text{Pa}]) = (28.2 \pm 0.5) - (11892 \pm 188)/T; \sigma = 3.2 \times 10^{-2}; r = 0.9989; n = 11.$

Table 7. Thermodynamic Characteristics of Sublimation and Fusion Processes of the Compounds Studied

VII	VIII	IX	X	XI	XII
$\Delta G_{\text{sub}}^0 [\text{kJ}\cdot\text{mol}^{-1}]$	60.8	62.6	64.5	60.2	60.4
$\Delta H_{\text{sub}}^T [\text{kJ}\cdot\text{mol}^{-1}]$	126.1 ± 2.1	116.3 ± 2.5	128.9 ± 2.5	134.8 ± 1.9	112.4 ± 2.1
$\Delta H_{\text{sub}}^0 [\text{kJ}\cdot\text{mol}^{-1}]$	129.0 ± 2.1	120.7 ± 2.5	132.6 ± 2.5	137.3 ± 1.9	115.6 ± 2.1
$C_{\text{p},\text{cr}}^{298} [\text{J}\cdot\text{mol}^{-1}\cdot\text{K}^{-1}]^a$	366.0	344.9	308.3	316.2	308.3
$T \cdot \Delta S_{\text{sub}}^0 [\text{kJ}\cdot\text{mol}^{-1}]$	68.2	58.1	68.1	77.1	55.2
$\Delta S_{\text{sub}}^0 [\text{J}\cdot\text{mol}^{-1}\cdot\text{K}^{-1}]$	229 ± 8	195 ± 8	228 ± 9	259 ± 8	185 ± 7
$T_{\text{fus}} [\text{K}]$	363.4 ± 0.2	402.3 ± 0.2	408.4 ± 0.2	361.5 ± 0.2	390.2 ± 0.2
$\Delta H_{\text{fus}}^T [\text{kJ}\cdot\text{mol}^{-1}]$	28.8 ± 0.5	29.6 ± 0.5	32.1 ± 0.5	26.8 ± 0.5	35.0 ± 0.5
$\Delta S_{\text{fus}}^T [\text{J}\cdot\text{mol}^{-1}\cdot\text{K}^{-1}]^b$	79 ± 3	74 ± 3	79 ± 3	74 ± 3	90 ± 3

<sup>a</sup> $C_{\text{p},\text{cr}}^{298}$  has been calculated by an additive scheme.<sup>23</sup> <sup>b</sup> $\Delta S_{\text{fus}}^T = \Delta H_{\text{fus}}^T/T_{\text{fus}}$ .

GAUSSIAN 03 at the MP2/6-31G\*\* level of theory. The electron density was then analyzed using the PIXEL module, which allows calculating lattice energies. The results of calculations are shown in Table 4S and Figure 2S (Supporting Information). According to PIXEL, electrostatic interactions contribute significantly into the calculated crystal lattice energies. Moreover, the Coulombic energy for certain molecules is equal or even greater than the dispersion energy. As it follows from Table 4S and Figure 2S, the PIXEL approach failed to predict the experimental values of crystal lattice energies even qualitatively. This fact may be caused by “poor accuracy” of the PIXEL calculation in this particular case. First of all, crystal lattice energy in the PIXEL approach refers to a transition of a rigid molecule from the crystal to the gas phase and does not include any intramolecular rearrangement energy. In addition, all the compounds studied are able to form multicentered hydrogen bonds in the crystal, which introduce an error at calculation of electrostatic energy. It is clear that an accurate calculation of energies of the intermolecular interactions for such complicated systems demands much more sophisticated quantum chemical methods, such as periodic DFT calculations with dispersion correction (DFT-D) or periodic MP2 calculations. An alternative way is to develop (or modify) the atom–atom potentials scheme for the thiadiazol compounds, which is based on experimental data. Therefore, in this paper we did not set ourselves task of

calculation of the all intermolecular interactions possible. Instead, we have been focused on the conformational energies, relationships between the molecular conformational flexibility and crystal structure, crystal structure, and sublimation thermodynamics. It turns out that the conformational preferences of thiadiazols play a crucial role at hydrogen bonds network organization in the crystals. Thus conformational energies should be taken into account for an accurate calculation of the crystal lattice energies.

It should be noted that the sublimation and thermophysical characteristics of the crystals are integral parameters which incorporate the sum of energy and structural changes of a system during phase transition. Therefore, it is difficult to highlight the influence of certain factors on the mentioned characteristics. It has been shown in our previous works that such descriptors as van der Waals molecular volume ( $V_{\text{vdw}}$ ), molecular free volume ( $V_{\text{free}}$ ) and their ratio ( $\beta = V_{\text{free}}/V_{\text{vdw}}$ ) may be useful enough to find out the relationship between the structural and thermodynamic parameters of crystals. The parameter  $\beta = V_{\text{free}}/V_{\text{vdw}}$  has been introduced for the description of the molecule packing density in the crystal. It is inversely proportional to the packing density and shows the change of the free volume per one molecule in the crystal when its van der Waals volume increases. Moreover, this approach allows us to analyze the effect of molecule topology and conformational state on the crystal packing architecture. For

example, the analysis of experimental values  $\beta$  versus  $V_{\text{vdw}}$  makes it possible to describe how much the molecular topology influences the packing characteristics in a crystal (Figure 16). It

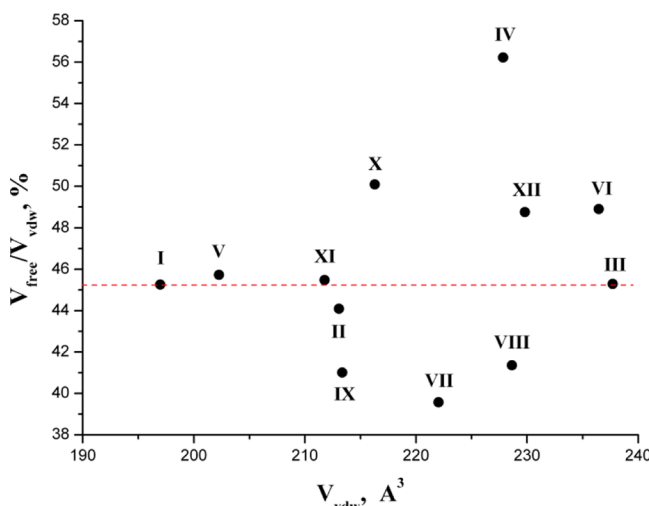


Figure 16. Plot of  $V_{\text{free}}/V_{\text{vdw}}$  versus  $V_{\text{vdw}}$  for the compounds studied. Numbering corresponds to Figure 1.

is notable that the molecule structural modification of I is accompanied by both an increase and a diminution in the packing density. For III, V, and XI, the gain of  $V_{\text{vdw}}$  is counterbalanced by the increase in  $V_{\text{free}}$  and the  $\beta$  parameter remains unchanged. One can notice that the presence of branched H-bond networks in a crystal usually diminishes the packing density of such compounds (IV, VI, X, and XI). First of all, it may be connected with the fact that the crystals are constructed from the conformationally “undesirable” molecules, the geometry of which is stabilized by strong hydrogen bonds. Moreover, in the crystal of IV, the molecular free volume reaches more than half of the van der Waals volume that leads to an anomalous decrease in the packing density.

The experimental values of  $\Delta H_{\text{sub}}^0$  as functions of  $\beta$  for the studied compounds are presented in Figure 17. The sublimation enthalpy and packing density corresponding to I

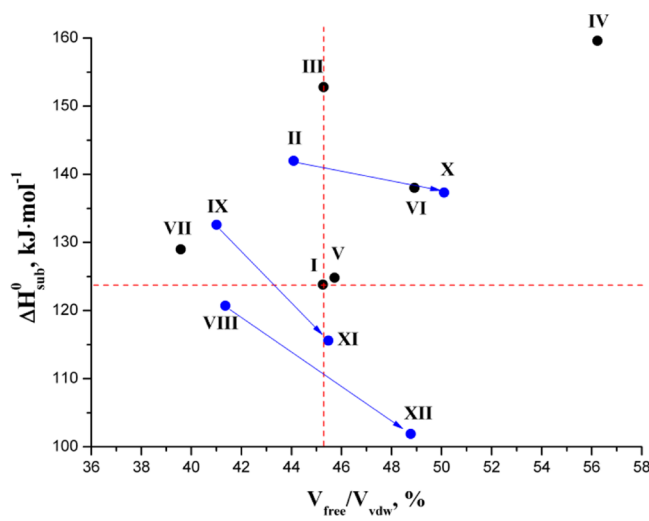


Figure 17. Plot of  $\Delta H_{\text{sub}}^0$  versus  $V_{\text{free}}/V_{\text{vdw}}$  ( $\beta$  parameter) for the compounds studied. Isomeric compounds are colored in blue for clarity. Numbering corresponds to Figure 1.

are depicted by horizontal and vertical lines, respectively. There is no correlation between these two parameters, though a number of regularities have to be mentioned. The analysis of compounds with branched H-bond organization of the crystal structure (IV, VI, and X) shows that the increase in  $\Delta H_{\text{sub}}^0$  is accompanied by a  $\beta$  parameter increase. On the other hand, for the compounds with  $\beta \leq \beta_1$  (II, VII, and IX), a gain of  $\Delta H_{\text{sub}}^0$ -values is also observed (except for VIII). We suppose that in the former the crystal lattice energy growth is provided by the strong H-bonds, while in the latter it is provided by the van der Waals interactions. The relationship between the packing density and the sublimation enthalpy is clearly illustrated by the example of isomeric compounds. As Figure 17 shows, for all the isomers,  $\Delta H_{\text{sub}}^0$ -values diminish as the  $\beta$  parameter increases (packing density decreases). It is worth mentioning that among the analyzed systems, XII has the minimal sublimation enthalpy as well as Gibbs energy. However, it is quite similar to IX in terms of crystal structure (see section 3.2. Crystal structure analysis). We believe that such difference of thermodynamic parameters may be attributed to the phenyl fragment conformational flexibility. In accordance with theoretical calculations, relatively low rotation energy barrier allows molecules of IX to adopt a more suitable conformation and, thus, a more compact packing. While for XII, the phenyl fragment deviation conformation is restricted because of the steric hindrance induced by the bulky methyl substituent.

In pharmaceutics, fusion temperature ( $T_{\text{fus}}$ ) is often applied as a parameter that indirectly specifies crystal lattice energy. It is due to the fact that the thermophysical parameters ( $T_{\text{fus}}$ ,  $\Delta H_{\text{fus}}^T$ ) can be easily obtained by the routine DSC method. As an example, it is necessary to mention the general solubility equation (GSE) derived by Yalkowsky and Valvani<sup>32</sup> which describes the solubility of poorly soluble drug compounds in water. To illustrate how this parameter ( $T_{\text{fus}}$ ) is handled in pharmaceutics, we tried to analyze this parameter by means of the above-mentioned  $\beta$  descriptor. The experimental  $T_{\text{fus}}$ -values as functions of  $\beta$  are illustrated in Figure 18. One can see that, for the majority of molecules, the increase in the fusion temperature is accompanied by a decrease in the  $\beta$  parameter. In case of IV and VI, the high  $T_{\text{fus}}$ -values with such “loose” packing may be explained by stabilization via strong H-bonds.

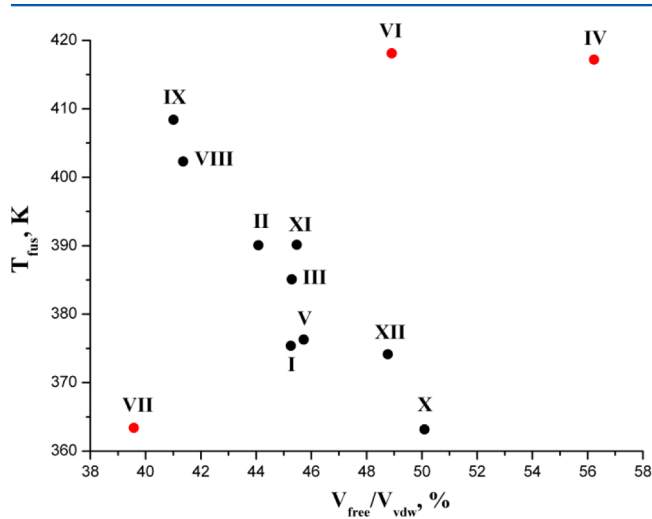


Figure 18. Plot of melting temperature versus  $V_{\text{free}}/V_{\text{vdw}}$  ( $\beta$  parameter) for the compounds studied. Numbering corresponds to Figure 1.

In fact, the structure of **IV** shows a unique organization of H-bond pattern, which consists of *S* and *R* enantiomers exclusively. In turn, compound **VI** is found to be the most thermally stable one due to an additional center of hydrogen bonding. On the contrary, the structure of **VII** shows the lowest  $T_{\text{fus}}$ -value among the thiadiazoles, although its packing density is rather high. It is hard to explain such behavior. It seems that a possible reason is the lack of close contacts, which are responsible for thermal stability of the crystal (as it has been shown in our previous papers).<sup>33</sup>

#### 4. CONCLUSION

The crystal structures of six thiadiazole derivatives (**VII–XII**) have been solved by X-ray diffraction experiments. It turns out that the presence of several sites of hydrogen bonding combined with conformational flexibility resulted in diversity of crystal structures. The DFT calculations show that conformational flexibility is a consequence of the relatively low rotation energy requirements of different parts of the molecules. Therefore, a wide set of conformations is available for packing during nucleation and new phase growth. Hydrogen bonds play a crucial role in this process. Hence, all the molecules were divided into two groups of conformations, namely anti and syn ones, depending on the relative position of the alcoholic proton (H1) and thiadiazole ring. The analysis of rotation energy profile reveals that the syn-configuration of OH group is metastable within the whole range of  $\tau_3$ -angle values. On the other hand, the molecule conformational strains are covered by a gain in the packing energy due to the additional H-bonds formation. Furthermore, the orientation of different fragments of the thiadiazole molecules in a crystal appears to be defined by the balance between the intermolecular interactions energy and the conformational strains energy. The rotation of the phenyl group requires the least amount of energy and, therefore, it is provided by weak van der Waals forces. However, a new hydrogen bond needs to be formed if rotation about  $\tau_2$ - and  $\tau_3$ -angles is necessary.

The molecule structural modification of **I** is accompanied by both an increase and a diminution in the packing density. The presence of branched H-bond networks in a crystal usually diminishes the packing density of such compounds (**IV**, **VI**, **X**, and **XI**).

The thermodynamic aspects of the thiadiazole sublimation processes have been studied by investigating the temperature dependence of vapor pressure by the transpiration method. A thermophysical study of fusion processes of the molecular crystals was carried out. It has been found that there is no correlation between the crystal lattice energy and the packing density of the studied compounds. However, for all the isomers, the  $\Delta H_{\text{sub}}^0$ -values diminish as the  $\beta$  parameter increases (the packing density decreases). The analysis of the thermophysical parameters of fusion processes shows that, for the majority of molecules, an increase in the fusion temperature is accompanied by a decrease in the  $\beta$  parameter (the packing density decreases).

#### ■ ASSOCIATED CONTENT

##### Supporting Information

Illustrations of the second level of H-bond motives occurring in crystals of the compounds studied, crystallographic data, saturation vapor pressure, and sublimation thermodynamics for compounds **I–VI**, crystal lattice energies of the compounds

studied calculated using PIXEL model. This material is available free of charge via the Internet at <http://pubs.acs.org>.

#### ■ AUTHOR INFORMATION

##### Corresponding Author

\*E-mail: glp@isc-ras.ru. Tel.: +7 4932 533784. Fax: +7 4932 336237.

##### Notes

The authors declare no competing financial interest.

#### ■ ACKNOWLEDGMENTS

This work was supported by the Federal Agency for Science and Innovations (No. 02.740.11.0857), the Russian Foundation of Basic Research (Nos. 12-03-00019, 13-03-00348), and the seventh framework program of the European Community for research, technological development and demonstration activities (IRSES-GA-2009-247500).

#### ■ REFERENCES

- (1) Li, Y.; Geng, J.; Liu, Y.; Yu, S.; Zhao, G. Thiadiazole - a Promising Structure in Medicinal Chemistry. *ChemMedChem* **2013**, *8*, 27–41.
- (2) Unangst, P. C.; Shrum, G. P.; Connor, D. T.; Dyer, R. D.; Schrier, D. J. Novel 1,2,4-Oxadiazoles and 1,2,4-Thiadiazoles as Dual 5-Lipoxygenase and Cyclooxygenase Inhibitors. *J. Med. Chem.* **1992**, *35*, 3691–3698.
- (3) Song, Y. T.; Connor, D. T.; Sercel, A. D.; Sorenson, R. J.; Doubleday, R.; Unangst, P. C.; Roth, B. D.; Beylin, V. G.; Gilbertsen, R. B.; Chan, K.; et al. Synthesis, Structure-Activity Relationships, and in Vivo Evaluations of Substituted Di-tert-butylphenols as a Novel Class of Potent, Selective, and Orally Active Cyclooxygenase-2 Inhibitors. 2. 1,3,4- and 1,2,4-Thiadiazole Series. *J. Med. Chem.* **1999**, *42*, 1161–1169.
- (4) Kohara, Y.; Kubo, K.; Imamiya, E.; Wada, T.; Inada, Y.; Naka, T. Synthesis and Angiotensin II Receptor Antagonistic Activities of Benzimidazole Derivatives Bearing Acidic Heterocycles as Novel Tetrazole Bioisosteres. *J. Med. Chem.* **1996**, *39*, 5228–5235.
- (5) Hara, R.; Sakamoto, K.; Hisamichi, H.; Nagano, N. Structure-activity Relationships of Cephalosporins Having a (Dimethylisoxazolidinio)vinyl Moiety at Their 3-Position. *J. Antibiot.* **1996**, *49*, 1162–1171.
- (6) Ishikawa, T.; Iizawa, Y.; Okonogi, K.; Miyake, A. Studies on anti-MRSA Parenteral Cephalosporins. I. Synthesis and Antibacterial Activity of 7 $\beta$ -[2-(5-amino-1,2,4-thiadiazol-3-yl)-2( $Z$ )-hydroxyiminoacetamido]-3-(substituted imidaz). *J. Antibiot.* **2000**, *53*, 1053–1070.
- (7) Castro, A.; Castan, T.; Encinas, A.; Porcal, W.; Gil, C. Advances in the Synthesis and Recent Therapeutic Applications of 1,2,4-Thiadiazole Heterocycles. *Bioorg. Med. Chem.* **2006**, *14*, 1644–1652.
- (8) Kumar, D.; Maruthi Kumar, N.; Chang, K. H.; Shah, K. Synthesis and Anticancer Activity of 5-(3-indolyl)-1,3,4-thiadiazoles. *Eur. J. Med. Chem.* **2010**, *45*, 4664–4668.
- (9) Macleod, A. M.; Baker, R.; Freedman, S. B.; Patel, S.; Merchant, K. J.; Roe, M.; Saunders, J. Synthesis and Muscarinic Activities of 1,2,4-Thiadiazoles. *J. Med. Chem.* **1990**, *33*, 2052–2059.
- (10) Martinez, A.; Fernández, E.; Castro, A.; Conde, S.; Rodríguez-Franco, I.; Baníos, J. E.; Badía, A. E. N-Benzylpiperidine Derivatives of 1,2,4-Thiadiazolidinone as New Acetylcholinesterase Inhibitors. *Eur. J. Med. Chem.* **2000**, *35*, 913–922.
- (11) Alonso, M.; Martinez, A. GSK-3 Inhibitors: Discoveries and Developments. *Curr. Med. Chem.* **2004**, *11*, 755–763.
- (12) Perlovich, G. L.; Proshin, A. N.; Volkova, T. V.; Petrova, L. N.; Bachurin, S. O. Novel 1,2,4-Thiadiazole Derivatives as Potent Neuroprotectors: Approach to Creation of Bioavailable Drugs. *Mol. Pharmaceutics* **2012**, *9*, 2156–2167.
- (13) Perlovich, G. L.; Bauer-Brandl, A. Solvation of Drugs as a Key for Understanding Partitioning and Passive Transport Exemplified by NSAIDs. *Curr. Drug Delivery* **2004**, *1*, 213–226.

- (14) Perlovich, G. L.; Volkova, T. V.; Proshin, A. N.; Sergeev, D. Y.; Bui, C. T.; Petrova, L. N.; Bachurin, S. O. Synthesis, Pharmacology, Crystal Properties, and Quantitative Solvation Studies from a Drug Transport Perspective for Three New 1,2,4-Thiadiazoles. *J. Pharm. Sci.* **2010**, *99*, 3754–3768.
- (15) Perlovich, G. L.; Proshin, A. N.; Volkova, T. V.; Bui, C. T.; Bachurin, S. O. Thermodynamic and Structural Aspects of Novel 1,2,4-Thiadiazoles in Solid and Biological Mediums. *Mol. Pharmaceutics* **2011**, *8*, 1807–1820.
- (16) Vivona, N.; Cusmano, G.; Macaluso, G. Mononuclear Heterocyclic Rearrangements. Rearrangements in the 1,2,4-Oxadiazoles, Isoxazoles, and 1,2,5-Oxadiazoles Involving a Sulphur Atom. *J. Chem. Soc., Perkin Trans. 1* **1977**, *1*, 1616–1619.
- (17) Boulton, J.; Katritzky, A. R.; Hamid, A. M. Heterocyclic Rearrangements. Part X. A Generalised Monocyclic Rearrangement. *J. Chem. Soc.* **1967**, 2005–2007.
- (18) Macaluso, G.; Cusmano, G.; Buscemi, S. Heterocyclic rearrangements. Rearrangements in the 1,2,4-Oxadiazoles, Isoxazoles, and 1,2,5-Oxadiazoles Involving a Carbethoxythiourea Nitrogen-Carbonsulfur Sequence. *Heterocycles* **1986**, *24*, 3433–3439.
- (19) CAD-4 Software, version 5.0; Enraf-Nonius: Delft, The Netherlands, 1989.
- (20) Sheldrick, G. M. *SHELXL97 and SHELXS97*; University of Göttingen: Germany, 1997.
- (21) Zielenkiewicz, W.; Perlovich, G. L.; Wszelaka-Rylik, M. The Vapour Pressure and the Enthalpy of Sublimation Determination by Inert Gas Flow method. *J. Therm. Anal. Calorim.* **1999**, *57*, 225–234.
- (22) Cox, J. D.; Pilcher, G. *Thermochemistry of Organic and Organometallic Compounds*; Academic Press: London, U.K., 1970.
- (23) Chickos, J. S.; Acree, W. E., Jr. Enthalpies of Sublimation of Organic and Organometallic Compounds. *J. Phys. Chem. Ref. Data.* **2002**, *31*, 537–698.
- (24) Surov, A. O.; Terekhova, I. V.; Bauer-Brandl, A.; Perlovich, G. L. Thermodynamic and Structural Aspects of Some Fenamate Molecular Crystals. *Cryst. Growth Des.* **2009**, *9*, 3265–3272.
- (25) Lee, C.; Yang, W.; Parr, R. G. Development of the Colle-Salvetti Correlation-energy Formula into a Functional of the Electron Density. *Phys. Rev. B* **1988**, *37*, 785–789.
- (26) Becke, A. D. Density Functional Calculations of Molecular Bond Energies. *J. Chem. Phys.* **1986**, *84*, 4524–4529.
- (27) Delley, B. An All-electron Numerical Method for Solving the Local Density Functional for Polyatomic Molecules. *J. Chem. Phys.* **1990**, *92*, 508–517.
- (28) Delley, B. Fast Calculation of Electrostatics in Crystals and Large Molecules. *J. Phys. Chem.* **1996**, *100*, 6107–6110.
- (29) Delley, B. From Molecules to Solids with the DMol<sup>3</sup> Approach. *J. Chem. Phys.* **2000**, *113*, 7756–7764.
- (30) Etter, M. C. Encoding and Decoding Hydrogen-bond Patterns of Organic Compounds. *Acc. Chem. Res.* **1990**, *23*, 120–126.
- (31) Bernstein, J.; Davis, R. E.; Shimoni, L.; Chang, N-L Patterns in Hydrogen Bonding: Functionality and Graph Set Analysis in Crystals. *Angew. Chem., Int. Ed. Engl.* **1995**, *34*, 1555–1573.
- (32) Yalkowsky, S. H.; Valvani, S. C. Solubility and Partitioning I: Solubility of Nonelectrolytes in Water. *J. Pharm. Sci.* **1980**, *69*, 912–922.
- (33) Perlovich, G. L.; Ryzhakov, A. M.; Tkachev, V. V.; Hansen, L. Kr. Sulfonamide Molecular Crystals: Thermodynamic and Structural Aspects. *Cryst. Growth Des.* **2011**, *11*, 1067–1081.
- (34) Gavezzotti, A. Efficient computer modeling of organic materials. The atom-atom, Coulomb-London-Pauli (AA-CLP) model for intermolecular electrostatic-polarization, dispersion and repulsion energies. *New J. Chem.* **2011**, *35*, 1360–1368.